Impact of velocity correlations on longitudinal dispersion in space-Lagrangian advective transport models

Tomás Aquino [1,*] and Andrés Velásquez-Parra [2,3]

[1]*Géosciences Rennes, UMR 6118, CNRS, Université de Rennes 1, 35000 Rennes, France*
[2]*Department of Water Resources and Drinking Water, Swiss Federal Institute of Aquatic Science and Technology, Eawag, 8600 Dübendorf, Switzerland*
[3]*Department of Civil, Environmental and Geomatic Engineering, ETH Zürich, CH-8093 Zürich, Switzerland*

Space-Lagrangian random walk models conceptualize advective transport in terms of collections of particles undergoing fixed-length steps along flow streamlines. The statistics and correlation structure of the underlying flow velocity statistics determine the transit times of particles undergoing advective transport. Broad velocity distributions lead to broadly distributed step transit times, reproducing commonly observed anomalous transport features such as superdiffusive plume growth, which are not captured by classical Fickian theories. Early space-Lagrangian models considered uncorrelated velocities across steps. These approaches were later extended to account for correlations through a spatial-Markov process. Here, we compare longitudinal dispersion dynamics in an uncorrelated continuous-time random walk with fixed-space steps to a Bernoulli relaxation spatial-Markov model exhibiting exponential decay of spatial velocity correlations along streamlines. We provide rigorous theoretical derivations, validated against numerical simulations. We find that, although the scaling forms of asymptotic dispersion agree between the two models, exact asymptotic equivalence requires employing different correlation lengths, which depend on the underlying Eulerian velocity statistics. The two models become equivalent in the limit of very broad velocity distributions, corresponding to a new quasiballistic regime recently identified in unsaturated porous media, which we rigorously characterize here.

I. INTRODUCTION

It is by now well known that transport in heterogeneous porous media often departs from classical Fickian dynamics [1–3]. Lagrangian random walk methods attempt to predict anomalous transport features, such as faster or slower plume dispersion and a preponderance of late arrivals at a control plane, by discretizing transported solute masses into a collection of particles undergoing movement according to stochastic rules. These rules encode the statistical variability of medium and flow properties in terms of the distribution of the duration and length of particle jumps [4,5].

In particular, this work is concerned with space-Lagrangian models, which conceptualize transport in terms of a series of fixed-size steps along the downstream (i.e., mean flow velocity) direction. Space-Lagrangian models can be subdivided into two main classes: continuous-time random walk (CTRW) models, where the duration of subsequent particle jumps are independent and identically distributed [1,6,7], and spatial-Markov models, where the statistics of these durations are conditioned on the previous jump due to velocity correlations [8–10]. The Markov property

---
*tomas.decamposaquino@univ-rennes1.fr

means that particle movement depends only on the current state, and not on previous history. While temporal dynamics have commonly been found to be non-Markovian, the dynamics in terms of fixed-spatial displacements can often be modeled as a Markov process [8,11–13]. This happens because natural media are often characterized by well-defined length scales, such as the grain or pore size at the pore scale or the extent of a geological feature at the Darcy scale. The long waiting times responsible for non-Markovian behavior typically result from localized slow movement in low-velocity (or low-permeability) regions. When considered as a function of time rather than distance from injection or number of spatial steps, the dynamics of spatial-Markov processes may be non-Markovian as a result of broadly distributed waiting times [9,14,15], thus allowing for modeling complex phenomena within a simpler framework. Indeed, anomalous transport resulting from advective variability has been successfully modeled with recourse to simple space-Markov processes at both the pore [16] and Darcy [17–19] scales. Although in this work we focus on purely advective transport models, we note that the effect of both transverse [20] and longitudinal [21–24] diffusion has also been considered in the context of spatial-Markov models. Diffusion, whether along or across streamlines, allows particles to more quickly escape low-velocity regions, leading to Fickian dispersion at sufficiently late times [21]. Spatial-Markov models based on small-scale numerical parametrization of the transit-time distributions have also been extensively employed to upscale conservative transport in porous [14,25] and fractured media [26,27], breakthrough curves in surface flows [28], and subsurface inertial and turbulent flows [29–31], as well as mixing and reaction [32–35].

In the context of purely advective transport, and in the absence of trapping due to zero-velocity regions or recirculation zones, the transit times of a space-Lagrangian model, representing the duration of each step, are directly related to the particle velocities during steps. They can thus be related to flow properties such as the average tortuosity, longitudinal velocity correlation length, and Eulerian point velocity statistics [16,36]. Uncorrelated (i.e., CTRW-type) space-Lagrangian models may be seen as a limiting case of spatial-Markov models, where velocities fully decorrelate between subsequent steps. It has been shown that both these and correlated spatial-Markov velocity models lead to either Fickian dispersion or superdiffusive behavior, i.e., superlinear growth of plume dispersion with time [20,36]. It is important to note that CTRW models which allow for symmetric backward and forward steps (as happens for regular diffusion), together with broad distributions of transit times, lead rather to subdiffusion, that is, sublinear temporal growth of plume dispersion [1,6,7,37,38]. Similarly, broad distributions of trapping times, with solute particles remaining immobile along the downstream direction, also lead to subdiffusion [39,40].

The purpose of this work is to compare the dispersion properties of correlated and uncorrelated space-Lagrangian models of advective transport. We focus on two fundamental models, namely, an uncorrelated continuous-time random walk (CTRW) and a spatial-Markov model with Bernoulli relaxation of velocities [16,20,36]. In order to render this work reasonably self-contained, as well as to collect relevant results found throughout the literature, we discuss the setup of these models and provide detailed derivations for asymptotic dispersion, tying its evolution to general features of the underlying Eulerian velocity distribution. As expected, our results agree with those previously reported for transit-time distributions decaying as a power law for the CTRW [41,42] and power-law behavior of the Eulerian velocity PDF at low velocities in both the CTRW and the Bernoulli model [17,36]. While the scalings for superdiffusive plume spreading have been shown to be equal in these two models for a number of cases [20,36], they have not been compared in detail. We also obtain explicit results for certain non-power-law forms of the Eulerian velocity probability density function (PDF) at low velocities. In particular, we identify a quasiballistic regime, associated with dispersion behavior that has been observed in the context of advective transport in unsaturated porous media [43]. In comparing the correlated and uncorrelated cases, we show that the Bernoulli relaxation spatial-Markov model exhibits larger dispersion than an uncorrelated CTRW that decorrelates on the same length scale. This means that, in order to render the two models fully equivalent regarding asymptotic dispersion, the step length of an uncorrelated CTRW for space-Lagrangian particle dynamics must be taken larger than the correlation length of the Bernoulli relaxation model, which

coincides with the correlation length of Lagrangian velocities along streamlines [16,36]. To the best of our knowledge, this surprising result has not been previously discussed in the literature. The relationship between correlation lengths depends on the low-velocity behavior of the underlying Eulerian velocity statistics. Dispersion in both models becomes independent of the correlation length in the quasiballistic limit that arises for a certain class of very broad velocity statistics.

The paper is structured as follows. The CTRW and Bernoulli relaxation models are introduced in Sec. II. The corresponding asymptotic dispersion dynamics are derived in Sec. III. Results are collected and overviewed at the end of this section, and are then validated against numerical simulations in Sec. IV. Conclusions are presented in Sec. V, and additional technical details on the derivations are presented in the Appendices.

II. SPACE-LAGRANGIAN TRANSPORT MODELS

In this section, we provide a brief review of space-Lagrangian models of advective transport, i.e., stochastic models characterized by fixed-length steps along particle trajectories (see also, e.g., [5,8,36]). For advective transport, the latter coincide with the flow streamlines. The corresponding velocity magnitudes V_n during each step n lead to a transit time $\tau_n = \ell/V_n$ across a step length ℓ. Thus, the position S_n along streamlines after n steps and the corresponding arrival time T_n obey the stochastic recursion relations

$$S_{n+1} = S_n + \ell, \qquad T_{n+1} = T_n + \frac{\ell}{V_n}. \tag{1}$$

The stochasticity is encoded in the velocities V_n, which are assumed to form a Markov chain. This means that the probability distribution of V_{n+1} may depend on the previous velocity V_n, but not on earlier velocities. Thus, the stochastic process V_n seen as a function of step number n is characterized by the family of transition PDFs $r(\cdot|v'; \ell)$, defined such that $r(v|v') dv$ is the probability that the next velocity V_{n+1} is between v an $v + dv$, given the current velocity $V_n = v'$. The form of $r(v|v'; \ell)$ for a given step length ℓ defines the space-Lagrangian model.

The central goal of space-Lagrangian models is to relate transport dynamics to statistical properties of the underlying medium, typically through the statistical properties of the corresponding velocity field. A key quantity of interest is the Eulerian velocity PDF p_E, which encodes the point statistics of velocity magnitudes. It is defined so that $p_E(v) dv$ is the probability that a randomly chosen location in the medium is characterized by a velocity magnitude v. In order to formalize this, let X be a homogeneously distributed random variable taking position values within a medium, and let $v_E(\cdot)$ be the Eulerian velocity field. Denoting average quantities by angled brackets, the Eulerian velocity PDF is then defined by

$$p_E(v) = \langle \delta[v - v_E(X)] \rangle, \tag{2}$$

where $\delta(\cdot)$ is the Dirac delta. This is the PDF of velocities associated with a homogeneous distribution of particles in the medium. The properties of this velocity PDF, and its relation to velocity gradients, are discussed in detail in [20].

If particles are spatially distributed proportionally to the local velocity, i.e., flux weighted, the associated velocity distribution is the flux-weighted Eulerian PDF,

$$p_F(v) = \frac{v}{\langle V_E \rangle} p_E(v), \tag{3}$$

where V_E is a random variable distributed according to the Eulerian velocity distribution, so that $\langle V_E \rangle = \langle v_E(X) \rangle$ is the average velocity in the medium. As we will see, the flux-weighted Eulerian PDF plays a central role in space-Lagrangian velocity models.

Typically, we are interested in displacements along the mean flow direction, which we must relate to the distance traveled along streamlines. After n steps, we approximate the former X_n, in terms of the latter S_n, through the average tortuosity χ, so that $X_n = S_n/\chi$. The average tortuosity may

be obtained in terms of flow properties only. Writing $\mathbf{V}_E$ for a vector random variable distributed according to the distribution of vectorial Eulerian velocities, with magnitude V_E and an orientation along the mean flow direction given by the unit vector $\boldsymbol{n}_f$, we have [44,45]

$$\chi = \frac{\langle V_E \rangle}{\langle \mathbf{V}_E \cdot \boldsymbol{n}_f \rangle}. \tag{4}$$

While a stochastic model allowing for variable tortuosity can be designed, the latter is typically not the main driver of variability regarding longitudinal positions. The assumption that the mean value may be used simplifies the model and reduces the necessary inputs to the Eulerian velocity PDF and velocity correlations across subsequent steps [16,20,36]. We consider an instantaneous injection at the origin $X_0 = 0$ at time $T_0 = 0$. The stochastic recursion relations for particle positions along the mean flow direction after n steps become

$$X_{n+1} = X_n + \frac{\ell}{\chi}, \qquad T_{n+1} = T_n + \frac{\ell}{V_n}. \tag{5}$$

The position $X(t)$ at time t is then obtained as the position at the end of the last step before t, plus displacement according to the current velocity up to t. More formally, this can expressed as

$$X(t) = X_{N(t)} + \frac{V_{N(t)}}{\chi}[t - T_{N(t)}], \tag{6}$$

where $N(t) = \sup_n\{n \mid T_n < t\}$ is the (stochastic) number of transitions completed by time t. We will now see how these concepts are particularized to obtain an uncorrelated CTRW description and a Bernoulli spatial-Markov model.

A. Uncorrelated velocities: Continuous-time random walk

We consider first a continuous-time random walk (CTRW) formulation of particle trajectories, with independent velocities across successive steps. Jumps correspond to displacements of one velocity decorrelation length ℓ_d along streamlines. Note that we use the term "decorrelation length" rather than the more common "correlation length" in the context of the CTRW in order to distinguish it from the correlation length of the Bernoulli relaxation model, to be introduced below. The stochastic recursion relations defining this model are given by Eq. (1) with $\ell = \ell_d$, with successive velocities taken as independent (no correlation) and identically distributed. Velocities then remain constant over one spatial step, so that particle velocities are fully correlated up to the decorrelation length ℓ_d, and then fully decorrelate. The recursion relations for longitudinal positions are

$$X_{n+1} = X_n + \frac{\ell_d}{\chi}, \qquad T_{n+1} = T_n + \frac{\ell_d}{V_n}. \tag{7}$$

Assuming ergodicity, in the sense that the statistical properties of velocities along each streamline match the velocity statistics across the spatial domain, along with incompressibility, so that additional retention effects do not arise, the appropriate distribution of the velocities V_n in order to reflect the underlying flow statistics is the flux-weighted Eulerian PDF p_F of Eq. (3) (see, e.g., [20,36]). To understand why, note that the amount of distance traveled by a particle in a given time window is proportional to the velocity v. The probability of a particle having velocity v after crossing ℓ_d in a given time is thus proportional to v, that is, flux weighted. In particular, the average of the time τ_n needed to complete the nth transition is then independent of n and given by

$$\langle \tau \rangle = \langle \tau_n \rangle = \left\langle \frac{\ell_d}{V_n} \right\rangle = \ell_d \int_0^\infty dv \, v^{-1} p_F(v) = \frac{\ell_d}{\langle V_E \rangle}, \tag{8}$$

which recovers the correct Eulerian mean velocity associated with the mean transition time. Correspondingly, the transition PDF for the spatial velocity process is

$$r(v|v'; \ell_d) = p_F(v), \tag{9}$$

independent of the velocity v' in the previous step. These considerations hold for steps $n \geqslant 1$. The distribution of initial velocities V_0 is determined by the initial solute configuration. For simplicity, we take the initial condition as flux weighted, so that V_n has the same distribution for all $n \geqslant 0$.

The CTRW description may also be recast in terms of the statistics of crossing times $\tau_n = \ell_d / V_n$ associated with a correlation length, rather than the statistics of velocity. Let ψ be the PDF of each independent and identically distributed τ_n, that is, $\psi(t)\,dt$ is the probability that a step has a duration between t and $t + dt$. In order for the two descriptions to be equivalent, we must have $|\psi(t)\,dt| = |p_F(v)\,dv|$ under the transformation of variables $t = \ell_d / v$, yielding [36]

$$\psi(t) = \frac{\ell_d \langle \tau \rangle}{t^3} p_E \left(\frac{\ell_d}{t} \right). \tag{10}$$

Note that $\langle \tau \rangle = \int_0^\infty dt\, t\, \psi(t) = \ell_d / \langle V_E \rangle$, in agreement with Eq. (8), and

$$\langle \tau^2 \rangle = \frac{\ell_d^2 \langle V_E^{-1} \rangle}{\langle V_E \rangle}. \tag{11}$$

Thus, the second moment is finite if and only if $\langle V_E^{-1} \rangle$ is finite.

B. Correlated velocities: Bernoulli relaxation process

For length scales below the decorrelation length, successive velocities are correlated, and a model involving correlations is necessary to describe transport at those scales. We will consider here the simplest such model, where velocities in space form a Markov process characterized by a constant probability of decorrelation $1/\ell_c$ per unit distance. In other words, the correlation structure along streamlines is exponential, with a mean correlation length ℓ_c. This Markov process is called Bernoulli relaxation [16,20,36]. For the discrete recursion relations for longitudinal position in terms of finite steps Δs, we write

$$X_{n+1} = X_n + \frac{\Delta s}{\chi}, \qquad T_{n+1} = T_n + \frac{\Delta s}{V_n}, \tag{12}$$

where now successive velocities are not independent but form a Markov chain.

The transition PDFs characterizing the Markov chain, that is, the probability of velocity $V_{n+1} = v$ given $V_n = v'$, are given independently of n by

$$r(v|v'; \Delta s) = e^{-\Delta s / \ell_c} \delta(v - v') + [1 - e^{-\Delta s / \ell_c}] p_F(v), \tag{13}$$

that is, the velocity remains the same with probability $\exp(-\Delta s / \ell_c)$, while otherwise a new velocity is sampled from the equilibrium PDF, which is given by the flux-weighted Eulerian PDF (3) as before. This formulation recovers the continuous Bernoulli process in the limit of $\Delta s \to 0$ or, in practice, for $\Delta s \ll \ell_c$. Thus, while for the uncorrelated CTRW the spatial step was equal to the decorrelation length ℓ_d, here the spatial step Δs is an arbitrary discretization used to resolve distances below the correlation length ℓ_c.

As for the (uncorrelated) CTRW, we focus on the case of a flux-weighted initial condition. The transit-time PDF across a correlation length ℓ_c is then given in Laplace space by [20,36]

$$\tilde{\psi}_B(\lambda) = \int_0^\infty dv\, \frac{p_F(v)}{1 + \ell_c \lambda / v}. \tag{14}$$

Here and throughout, we denote Laplace transforms with respect to time by a tilde, and the corresponding Laplace variable by λ. Note that ψ_B differs from the transit-time PDF ψ of the CTRW even for $\ell_d = \ell_c$ because there is now a nonzero probability of particle velocities changing before, or not changing after, traversing a correlation length. Denoting the random time to cross a correlation

length ℓ_c by τ_B, we find, using $d\tilde{\psi}_B(\lambda)/d\lambda|_{\lambda=0} = -\langle\tau_B\rangle$ and integration by parts,

$$\langle\tau_B\rangle = \frac{\ell_c}{\langle V_E\rangle}. \tag{15}$$

As expected, this result is equivalent to that for a CTRW with $\ell_d = \ell_c$ [see Eq. (8)]. However, the second moment of the transit times differs from that of Eq. (11) with $\ell_d = \ell_c$. It is given, when $\langle V_E^{-1}\rangle$ is finite, by

$$\langle\tau_B^2\rangle = \frac{2\ell_c^2\langle V_E^{-1}\rangle}{\langle V_E\rangle}, \tag{16}$$

which is exactly twice the CTRW value for the same Eulerian velocity distribution and $\ell_d = \ell_c$. As before, if $\langle V_E^{-1}\rangle$ diverges, so does $\langle\tau_B^2\rangle$, and transport is anomalous. If $\langle V_E^{-1}\rangle$ is finite, this means that the Bernoulli relaxation process leads to larger variability in crossing times.

III. DISPERSION

We will now use these formulations to compute late-time longitudinal dispersion. Longitudinal dispersion $\sigma^2(t)$ is defined as the variance of particle positions $X(t)$ as a function of time t, that is,

$$\sigma^2(t) = \langle X^2(t)\rangle - \langle X(t)\rangle^2. \tag{17}$$

Because the displacement in a given step is always ℓ_d/χ for the CTRW and $\Delta s/\chi$ for the Bernoulli relaxation model, when computing late-time dispersion we can approximate $X(t) \approx X_{N(t)}$ [see Eq. (6)]. For the correlated model, this approximation becomes exact at all times in the limit of small step Δs. However, for the CTRW model, interpolation of particle positions between steps according to Eq. (6) is necessary in order to capture early-time dispersion. Indeed, for small times t compared to the mean transit time, few transitions have occurred, so that most particles retain the initial velocity V_0, and $X(t) \approx V_0 t$. Thus,

$$\sigma^2(t) \approx \sigma_{V_0}^2 t^2, \tag{18}$$

where $\sigma_{V_0}^2 = \langle V_0^2\rangle - \langle V_0\rangle^2$, i.e., dispersion is ballistic at early times and determined by the variance of the initial velocity distribution. For a flux-weighted initial condition, the initial velocity V_0 is distributed according to the flux-weighted Eulerian PDF. Using the definition of the latter, Eq. (3), we then have

$$\sigma_{V_0}^2 = \left(\frac{\langle V_E^3\rangle}{\langle V_E\rangle^3} - \frac{\langle V_E^2\rangle^2}{\langle V_E\rangle^4}\right)\langle V_E\rangle^2. \tag{19}$$

Depending on the underlying velocity statistics, the late-time behavior of dispersion may be Fickian [$\sigma^2(t) \propto t$] or non-Fickian, more specifically superdiffusive [$\sigma^2(t)$ growing faster than t] [36]. The precise behavior depends on the velocity correlation structure. In what follows, we will employ two different quantitative approaches for the cases without and with correlations between subsequent steps. The results for the asymptotic scaling behavior are collected in Table I at the end of this section.

A. Continuous-time random walk

We now provide derivations of asymptotic dispersion for the CTRW considered here, relying on the fact that the step size ℓ_d is deterministic and time independent. For similar derivations of the relationship between dispersion and transit-time distribution accounting for distributed step sizes with finite and positive mean and variance, we refer the reader to [41,42]. For a treatment of dispersion in terms of the velocity correlation structure, see [36].

TABLE I. Asymptotic dispersion, associated with different Eulerian velocity PDFs, for the CTRW and Bernoulli relaxation models. The first column describes the scaling behavior of the Eulerian velocity PDF $p_E(v)$ at low velocities v; the second lists the qualitative type of asymptotic dispersion; the third shows the asymptotic scaling form of dispersion $\sigma^2(t)$; and the final two columns list the corresponding equations.

Eulerian PDF at low velocities v	Type	Temporal scaling	Eqs. (CTRW)	Eqs. (Bernoulli)
Finite $\langle V_E^{-1} \rangle$	Fickian	$\sim t$	(29)	(53)
$\sim v^0$	Superdiffusive (quasi-Fickian)	$\sim t \ln t$	(39), (44)	(60), (63)
$\sim v^\alpha,\ -1 < \alpha < 0$	Superdiffusive (power law)	$t^{1+|\alpha|}$	(34)	(57)
$\sim v^{-1} \ln^{-1-\alpha},\ \alpha > 0$	Superdiffusive (quasiballistic)	$t^2 \ln^{-1-\alpha} t$	(48)	(67)

As discussed above, in order to compute asymptotic dispersion for the CTRW, it suffices to assume that particles wait at a turning point for the duration τ_n of each step, and then transition instantaneously to $X_{n+1} = X_n + \ell$ at time T_{n+1}. The position as a function of time for the CTRW may then be approximated as

$$X(t) \approx X_{N(t)} = \chi^{-1} \ell_d N(t), \tag{20}$$

so that, according to Eq. (17),

$$\sigma^2(t) \approx \chi^{-2} \ell_d^2 \sigma_N^2(t), \tag{21}$$

where $\sigma_N^2(t) = \langle N^2(t) \rangle - \langle N(t) \rangle^2$ is the variance of the number of steps $N(t)$ completed by time t. This result simply states that, since there is no variability in the spatial steps, the variability in positions is controlled by the variability in number of steps by a given time. As shown in Appendix A, the Laplace transforms of the relevant moments can be expressed exactly in terms of the transit-time PDF as

$$\langle \tilde{N}(\lambda) \rangle = \frac{\lambda^{-1} \tilde{\psi}(\lambda)}{1 - \tilde{\psi}(\lambda)}, \tag{22a}$$

$$\langle \widetilde{N^2}(\lambda) \rangle = \frac{\tilde{\psi}(\lambda)}{\lambda} \frac{1 + \tilde{\psi}(\lambda)}{[1 - \tilde{\psi}(\lambda)]^2}. \tag{22b}$$

In order to obtain the late-time behavior of these moments, we consider the small-λ (large-time) expansion of $\tilde{\psi}(\lambda)$. The large-time limit is controlled by low velocities. Consider a Eulerian velocity PDF such that, for low velocities, $p_E(v) \propto v^\alpha$ for some power-law exponent α. According to Eq. (10), the transit times have a large-time tail $\propto t^{-3-\alpha}$. The Laplace expansion of the transit times is therefore

$$\tilde{\psi}(\lambda) \approx 1 - \langle \tau \rangle \lambda + \frac{(t_\beta \lambda)^\beta}{\Gamma(\beta + 1)}, \tag{23}$$

where $\beta = \min\{2, 2 + \alpha\}$ and $\Gamma(\cdot)$ is the gamma function. If the variance of the waiting times (or, equivalently, their second moment) is finite, which happens for $\alpha > 0$, then $\beta = 2$ and $t_2 = \sqrt{\langle \tau^2 \rangle}$. Otherwise, t_β is a characteristic timescale such that, for large $t \gg \langle \tau \rangle$,

$$\psi(t) \approx \frac{\sin(|\beta|\pi)}{\pi} t_\beta^\beta t^{-1-\beta}. \tag{24}$$

For a general discussion of the Laplace transform of heavy-tailed PDFs, see, e.g., [46,47]. Integrability of the velocity PDF near $v = 0$ requires $\alpha > -1$, so that we have $1 < \beta < 2$. Therefore, as expected, the mean waiting time is always finite; it is given by $\langle \tau \rangle = \ell_d / \langle V_E \rangle$ as already discussed [see Eq. (8)]. Note that additional corrections occur in the Laplace expansion when $\alpha = 0$ and $\psi(t) \propto t^{-3}$. The exact nature of the corrections depends on the velocity distribution. Additional

corrections also appear if the behavior of $p_E(v)$ is not a pure power law near $v = 0$. We will consider explicit examples below.

Inverting the Laplace transform in Eq. (22a) for small λ, according to Eq. (23) for $\tilde{\psi}(\lambda)$, leads to

$$\langle N(t) \rangle \approx \frac{t}{\langle \tau \rangle} + \frac{t_\beta^\beta}{\Gamma(3 - \beta)\Gamma(\beta + 1)\langle \tau \rangle^2} t^{2-\beta} - 1. \tag{25}$$

As expected, $\langle X(t) \rangle = \chi^{-1}\ell_d\langle N(t) \rangle \approx \langle V_E \rangle t$ to leading order in large time. For the second moment, inverting Eq. (22b) results in

$$\langle N^2(t) \rangle \approx \frac{t^2}{\langle \tau \rangle^2} + \frac{4t_\beta^\beta}{\Gamma(4 - \beta)\Gamma(\beta + 1)\langle \tau \rangle^3} t^{3-\beta} - \frac{3t}{\langle \tau \rangle}. \tag{26}$$

These results lead, according to Eq. (21), to the late-time dispersion

$$\sigma^2(t) \approx \frac{\ell_d^2}{\chi^2 \langle \tau \rangle} \left(\frac{2t_\beta^\beta}{\beta \Gamma(4 - \beta)\Gamma(\beta - 1)\langle \tau \rangle^2} t^{3-\beta} - t \right). \tag{27}$$

Note how the leading-order contribution, which would be $\propto t^2$ (i.e., ballistic), cancels out between the second moment and the square of the mean. This phenomenon is characteristic of dispersion in space-Lagrangian models.

1. Fickian dispersion

Consider now the case $\alpha > 0$, for which, as discussed, the transit times have a finite variance. In that case, $\beta = 2$, and Eq. (27) becomes

$$\sigma^2(t) \approx \frac{\ell_d^2}{\chi^2 \langle \tau \rangle} \left(\frac{\langle \tau^2 \rangle}{\langle \tau \rangle^2} - 1 \right) t. \tag{28}$$

Using Eqs. (8) and (11), this becomes, in terms of Eulerian velocity moments,

$$\sigma^2(t) \approx \frac{\ell_d \langle V_E \rangle}{\chi^2} \left(\langle V_E^{-1} \rangle \langle V_E \rangle - 1 \right) t. \tag{29}$$

Dispersion is thus Fickian, i.e., proportional to t as for regular diffusion. Note that this result is independent of the existence of non-power-law behavior of $p_E(v)$ near $v = 0$, so long as $\langle V_E^{-1} \rangle$, and therefore $\langle \tau^2 \rangle$, is finite.

2. Superdiffusion

For $-1 < \alpha < 0$, so that $1 < \beta = 2 + \alpha < 2$, the transit times have an infinite variance. This means that larger and larger variability in the waiting times is sampled as time increases [1,46]. The physical origin of this large variability is a strong preponderance of arbitrarily small velocities compared to the mean, corresponding to arbitrarily long times to cross a decorrelation length, over which velocities persist. For $\alpha \leqslant 0$, the relative importance of such velocities is sufficient to avoid convergence of the second moment of transit times. In this case, Eq. (27) yields the late-time behavior

$$\sigma^2(t) \approx \frac{2\ell_d^2}{\chi^2 \langle \tau \rangle^3} \frac{t_\beta^\beta}{\beta \Gamma(4 - \beta)\Gamma(\beta - 1)} t^{3-\beta}. \tag{30}$$

We now write the low-velocity behavior of the Eulerian PDF as

$$p_E(v) \approx \frac{c_\alpha}{\langle V_E \rangle} \left(\frac{v}{\langle V_E \rangle} \right)^\alpha, \tag{31}$$

for some dimensionless coefficient $c_\alpha > 0$. Note that any Eulerian PDF behaving as a power law near the origin can be expressed in this manner. The exponent α and the leading coefficient c_α determine the value of the characteristic time t_β, which impacts asymptotic dispersion according to Eq. (30). Indeed, according to Eq. (10), we have the transit-time PDF

$$\psi_B(t) \approx \frac{c_\alpha}{\langle \tau \rangle} \left(\frac{t}{\langle \tau \rangle} \right)^{-(3-|\alpha|)}, \tag{32}$$

and, using Eq. (24), we obtain

$$t_\beta = \left[\frac{c_\alpha \pi}{\sin(|\alpha|\pi)} \right]^{1/\beta} \langle \tau \rangle. \tag{33}$$

Substituting in Eq. (30) for dispersion and using the reflection identity $\Gamma(z)\Gamma(1 - z) = \pi / \sin(\pi z)$ for arbitrary noninteger z, we obtain, in terms of Eulerian velocity properties,

$$\sigma^2(t) \approx \frac{2c_\alpha \ell_d^{1-|\alpha|} \langle V_E \rangle^{1+|\alpha|}}{(2 - |\alpha|)(1 + |\alpha|)|\alpha|\chi^2} t^{1+|\alpha|}. \tag{34}$$

This corresponds to superdiffusive behavior, with dispersion growing as a power of time (strictly) between 1 and 2.

The edge case $\alpha = 0$ must be treated separately. First, consider the exponential Eulerian PDF

$$p_E(v) = \frac{e^{-v/\langle V_E \rangle}}{\langle V_E \rangle}, \tag{35}$$

which, according to Eq. (10), corresponds to the transit-time PDF

$$\psi(t) = \frac{\langle \tau \rangle^2}{t^3} e^{-\langle \tau \rangle/t}. \tag{36}$$

This has Laplace transform

$$\tilde{\psi}(\lambda) = 2\langle \tau \rangle \lambda K_2(2\sqrt{\langle \tau \rangle \lambda}), \tag{37}$$

where K_2 is the modified Bessel function of the second kind. For small $\lambda \ll 1/\langle \tau \rangle$,

$$\tilde{\psi}(\lambda) \approx 1 - \langle \tau \rangle \lambda - \frac{(\langle \tau \rangle \lambda)^2}{2} \ln \left(e^{2\gamma_E - 3/2} \langle \tau \rangle \lambda \right), \tag{38}$$

where $\gamma_E \approx 0.577$ is the Euler-Mascheroni constant. Using Eqs. (21) and (22) as before, we obtain

$$\sigma^2(t) \approx \frac{\ell_d \langle V_E \rangle}{\chi^2} t \, \ln \left(\frac{\langle V_E \rangle t}{e^{\gamma_E + 3/2} \ell_d} \right). \tag{39}$$

We note that multiplying the argument of the logarithm by a positive dimensionless constant does not affect the asymptotics at sufficiently late times, but may provide better estimates at earlier times. When the full analytical Laplace transform of the transit-time PDF is known, a constant that provides good results at earlier times may sometimes be found analytically, which is the case here.

Next, we consider a more general class of Eulerian PDFs scaling as $\sim v^0$, such that, for low velocities $v \ll \langle V_E \rangle$ compared to the mean velocity,

$$p_E(v) \approx \frac{c_1}{\langle V_E \rangle} \left[1 - \left(1 + \ln \left[\frac{c_3 v}{\langle V_E \rangle} \right] \right) \frac{c_2 v}{\langle V_E \rangle} \right] \tag{40}$$

for dimensionless coefficients $c_1, c_2, c_3 > 0$. This form arises as an approximation for the Eulerian PDF of saturated flow in $2d$ porous media [43], as discussed in more detail in Sec. IV B. According

to Eq. (10), we then have, for large times $t \gg \langle\tau\rangle$,

$$\psi(t) \approx \frac{c_1\langle\tau\rangle^2}{t^3}\left[e^{-c_2\langle\tau\rangle/t} + \frac{c_2\langle\tau\rangle}{t}\ln\left(\frac{t}{c_3\langle\tau\rangle}\right)\right]. \tag{41}$$

As for the exponential Eulerian PDF, $\langle V_E^{-1}\rangle$ diverges, so that $\langle\tau^2\rangle$ also diverges. The logarithmic term multiplied by t^2 is integrable at infinity, and therefore its Laplace expansion is a regular power series through second order in small λ. Since we know the zeroth-order term in the expansion of $\tilde{\psi}(\lambda)$, which is unity by normalization, and the coefficient of the first-order term, which is the mean time $\langle\tau\rangle$, the next leading term corresponding to the infinite second moment of this distribution must arise from the exponential term in parentheses. Indeed, the Laplace transform of $c_1\langle\tau\rangle^2 t^{-3}\exp(-c_2\langle\tau\rangle/t)$ is, similarly to the exponential case treated above, given by

$$\frac{2c_1\langle\tau\rangle\lambda K_2(2\sqrt{c_2\langle\tau\rangle\lambda})}{c_2} \approx \frac{c_1}{c_2^2} - \frac{c_1\langle\tau\rangle\lambda}{c_2} - \frac{c_1(\langle\tau\rangle\lambda)^2}{2}\ln\left(c_2 e^{2\gamma_E - 3/2}\langle\tau\rangle\lambda\right), \tag{42}$$

where the approximation holds for small $\lambda \ll 1/\langle\tau\rangle$. We thus conclude that

$$\tilde{\psi}(\lambda) \approx 1 - \langle\tau\rangle\lambda - \frac{c_1(\langle\tau\rangle\lambda)^2}{2}\ln\left(\langle\tau\rangle\lambda\right). \tag{43}$$

Note that in this case the factor inside the logarithm cannot be accurately determined without knowledge of the full form of the Eulerian PDF. However, it does not affect late-time dispersion, but only the onset of the scaling behavior. Using the same techniques as before, we find the leading-order dispersion behavior

$$\sigma^2(t) \approx \frac{c_1\ell_d\langle V_E\rangle}{\chi^2}t\,\ln\left(\frac{\langle V_E\rangle t}{\ell_d}\right). \tag{44}$$

In particular, this derivation shows that, for a Eulerian PDF behaving like $c_1(1 + c_2 v/\langle V_E\rangle)/\langle V_E\rangle$ near the origin, logarithmic corrections to the contributions linear in v and the value of c_2 do not affect asymptotic dispersion. In other words, the $t\ln t$ scaling behavior of dispersion for Eulerian PDFs behaving as $\sim v^0$ near the origin is robust and not limited to the exponential PDF. Note also that the result for the latter, Eq. (39), is recovered by setting $c_1 = 1$, up to the factor inside the logarithm as explained above.

When in the same advective transport problem just discussed the flow is unsaturated, the low-velocity behavior of the Eulerian PDF can instead be approximated by [43]

$$p_E(v) \approx c_\alpha v^{-1}\ln^{-1-\alpha}(v_c/v), \tag{45}$$

for small velocities compared to a characteristic velocity v_c. Here, $c_\alpha > 0$ is a dimensionless coefficient and $\alpha > 0$ is related to the tailing of the PDF of dead-end (i.e., regions of low liquid flow velocity) area sizes, $p_A(A) \propto A^{-1-\alpha/2}$, as discussed in more detail in Sec. IV B. Note that the logarithmic factor renders the PDF integrable near the origin. In this case, for large times compared to $t_d = \ell_d/v_c$, the large-time tailing behavior of the transit time PDF is, according to Eq. (10),

$$\psi(t) \approx c_\alpha\langle\tau\rangle t^{-2}\ln^{-1-\alpha}(t/t_d), \tag{46}$$

and the corresponding Laplace transform for small $\lambda \ll 1/t_d$ is

$$\tilde{\psi}(\lambda) \approx 1 - \langle\tau\rangle\lambda\left[1 - \frac{c_\alpha}{\alpha}\ln^{-\alpha}\left(\frac{1}{t_d\lambda}\right) - c_\alpha\frac{1 + \alpha\gamma_E}{\alpha}\ln^{-1-\alpha}\left(\frac{1}{t_d\lambda}\right)\right], \tag{47}$$

as shown in Appendix B. As before, the term proportional to λ corresponds to the (finite) mean waiting time $\langle\tau\rangle$. The next-order logarithmic correction is directly due to the tailing behavior; it is of lower order than λ^2, reflecting the nonexistence of the second moment. Finally, $\tilde{\psi}(0) = 1$ is the unit-integral normalization condition characteristic of all PDFs. Note that, as in the previous case, the exact coefficient inside the logarithm, which does not impact asymptotic dispersion, depends

on the full Eulerian PDF and cannot be accurately determined without its knowledge. As shown in Appendix B, we have in this case

$$\sigma^2(t) \approx \frac{c_\alpha \langle V_E \rangle^2}{\chi^2} t^2 \ln^{-1-\alpha}\left(\frac{v_d t}{\ell_d}\right). \tag{48}$$

This result describes quasiballistic behavior; dispersion slows down compared to the ballistic t^2 scaling only logarithmically. It presents the interesting feature that the asymptotic behavior is independent of the decorrelation length ℓ_d since the coefficient $v_d/\ell_d = 1/t_d$ within the logarithm does not affect dispersion at sufficiently late times $t \gg t_d$.

B. Bernoulli relaxation

In order to compute asymptotic dispersion under the Bernoulli model, we rely on the computation of velocity correlations. The techniques employed here follow those of [36]. We first express particle positions as a function of time as $X(t) = \chi^{-1} \int_0^t dt'\, V_T(t')$, where V_T is the time-Lagrangian velocity, that is, the velocity of Lagrangian particles along streamlines seen as a function of time. Directly computing the first and second moments, we obtain the Kubo-Green formula for advective dispersion [48]:

$$\frac{\chi^2 \sigma^2(t)}{\ell_c^2} = I_2(t) - I_1^2(t), \tag{49}$$

where

$$I_1(t) = \ell_c^{-1} \int_0^t dt'\, \langle V_T(t') \rangle, \tag{50a}$$

$$I_2(t) = \ell_c^{-2} \int_0^t dt' \int_0^t dt''\, \langle V_T(t') V_T(t'') \rangle. \tag{50b}$$

This means that velocity variability induces dispersion according to the correlation function of velocity fluctuations. Comparing to Eq. (21) for the CTRW, we see that dispersion in the Bernoulli relaxation model is equivalent to a CTRW with numbers of transitions by time t with variance $\sigma_N^2(t) = I_2(t) - I_1^2(t)$.

As shown in Appendix C, we have

$$\tilde{I}_1(\lambda) = \frac{\lambda^{-1} \tilde{\psi}_B(\lambda)}{1 - \tilde{\psi}_B(\lambda)}, \tag{51a}$$

$$\tilde{I}_2(\lambda) \approx \frac{2}{\lambda} \frac{1 - 2\langle \tau_B \rangle \lambda}{[1 - \tilde{\psi}_B(\lambda)]^2}. \tag{51b}$$

Note that Eq. (51a) is identical to Eq. (22a) for the average number of CTRW transitions upon replacing $\tilde{\psi}(\lambda)$ by $\tilde{\psi}_B(\lambda)$. In particular, we always have $\langle X(t) \rangle = I_1(t) \approx \langle V_E \rangle t$ to leading order at late times $t \gg \langle \tau_B \rangle$, as expected. Equation (51b) should be compared to Eq. (22b). Note that this form preserves the dependency in small $\lambda \ll 1/\langle \tau_B \rangle$ up to the necessary order to calculate dispersion to leading order in large times $t \gg \langle \tau_B \rangle$.

1. Fickian dispersion

The calculation of late-time dispersion now proceeds similarly to the CTRW case. When the second moment of the transit times exists, we expand $\tilde{\psi}_B(\lambda)$ for $\lambda \ll 1/\langle \tau_B \rangle$ as

$$\tilde{\psi}_B(\lambda) \approx 1 - \langle \tau_B \rangle \lambda + \frac{\langle \tau_B^2 \rangle}{2} \lambda^2, \tag{52}$$

with the first and second moments given by Eqs. (15) and (16). Expanding Eqs. (51) for small λ, inverting the Laplace transforms, and substituting in Eq. (49), we obtain

$$\sigma^2(t) \approx \frac{2\ell_c \langle V_E \rangle}{\chi^2} \big(\langle V_E^{-1} \rangle \langle V_E \rangle - 1 \big) t. \tag{53}$$

Thus, late-time dispersion is Fickian as expected. However, comparison to the corresponding equation for the CTRW [Eq. (29)], shows that the leading coefficients are equal only upon setting

$$\ell_d = 2\ell_c. \tag{54}$$

For $\ell_d = \ell_c$, the Bernoulli relaxation model exhibits twice the asymptotic dispersion of the CTRW. While one might think that this surprising result follows directly from the fact that the second moment of the transit times is twice as large for the Bernoulli process when $\ell_d = \ell_c$, this is not the case since the equivalence result for dispersion does not follow from simply replacing $\langle \tau^2 \rangle$ by $\langle \tau_B^2 \rangle = 2\langle \tau^2 \rangle$ in Eq. (29) while retaining $\ell_d = \ell_c$. Rather, as done here, the different correlation structures must be taken into account in more detail.

2. Superdiffusion

When the second moment $\langle \tau_B^2 \rangle$ is infinite, we must turn to the tailing behavior of $\psi_B(t)$ for large times, as for the CTRW model. Recognizing the λ-dependent part of the integrand as the Laplace transform of an exponential density, we invert Eq. (14) to obtain

$$\psi_B(t) = \ell_c^{-1} \int_0^\infty dv \, v p_F(v) e^{-vt/\ell_c}. \tag{55}$$

In the following, we consider the tailing of the transit-time PDF separately for different low-velocity behaviors of the Eulerian PDF. First, consider a Eulerian velocity PDF scaling as a power law $\sim v^\alpha$, $-1 < \alpha < 0$, near the origin [Eq. (31)]. For large times, the integral in Eq. (55) is dominated by the low-velocity contribution of $p_E(v)$. Solving the resulting integral, we obtain, for $t \gg \langle \tau_B \rangle$,

$$\psi_B(t) \approx \frac{c_\alpha \Gamma(3 - |\alpha|)}{\langle \tau_B \rangle} \left(\frac{t}{\langle \tau_B \rangle} \right)^{-(3-|\alpha|)}. \tag{56}$$

Comparing to Eq. (32), we conclude that the tailing behavior of the transit time PDF has the same scaling behavior as for the CTRW, but is larger by a factor of $\Gamma(3 - |\alpha|)$ when $\ell_c = \ell_d$. Proceeding as for the CTRW, but using Eqs. (49) and (51), we find the asymptotic dispersion

$$\sigma^2(t) \approx \frac{2c_\alpha \Gamma(3 - |\alpha|)\ell_c^{1-|\alpha|} \langle V_E \rangle^{1+|\alpha|}}{(2 - |\alpha|)(1 + |\alpha|)|\alpha|\chi^2} t^{1+|\alpha|} \tag{57}$$

[compare Eq. (34)]. We conclude that, while the scaling form with time is equivalent to the CTRW case, asymptotic equivalence of the two models regarding dispersion requires setting

$$\ell_d = \Gamma(3 - |\alpha|)^{1/(1-|\alpha|)} \ell_c. \tag{58}$$

The value of ℓ_d/ℓ_c varies between $e^{1-\gamma_E} \approx 1.526$ as $\alpha \to -1$ and 2 as $\alpha \to 0$. Correspondingly, for $\ell_d = \ell_c$, dispersion in the Bernoulli model is higher by a factor between 1 and 2.

As before, the edge case $\alpha = 0$ must be treated separately. We consider first the case of an exponential distribution of Eulerian velocities [Eq. (35)]. Performing the integration in Eq. (14) yields

$$\tilde{\psi}_B(\lambda) = 1 - \langle \tau_B \rangle \lambda - \langle \tau_B \rangle^2 e^{\langle \tau_B \rangle \lambda} \Gamma(0, \langle \tau_B \rangle \lambda)$$
$$\approx 1 - \langle \tau_B \rangle \lambda - (\langle \tau_B \rangle \lambda)^2 \ln (e^{\gamma_E} \langle \tau_B \rangle \lambda), \tag{59}$$

where $\Gamma(\cdot, \cdot)$ is the upper incomplete gamma function, $\Gamma(a, z) = \int_z^\infty dx \, x^{a-1} e^{-x}$, and the approximation holds for small $\lambda \ll 1/\langle \tau_B \rangle$. This result should be compared to Eq. (38). The same procedure

as above now yields

$$\sigma^2(t) \approx \frac{2\ell_c \langle V_E \rangle}{\chi^2} t \, \ln\left(\frac{\langle V_E \rangle t}{e^3 \ell_c}\right). \tag{60}$$

Comparison to Eq. (39) shows that equivalence to the CTRW at sufficiently late times requires setting $\ell_d = 2\ell_c$, as for the Fickian case.

Next, we consider the Eulerian PDF be given by Eq. (40), which corresponds to a logarithmic correction to flat power-law behavior near $v = 0$. In this case, performing the integral in Eq. (55) for the low-v dependency of $p_E(v)$, we obtain for $t \gg \langle \tau_B \rangle$

$$\psi_B(t) \approx \frac{2c_1 \langle \tau_B \rangle^2}{t^3} \left[e^{-c_2 \langle \tau_B \rangle / t} + \frac{3c_2 \langle \tau_B \rangle}{t} \ln\left(\frac{e^{\gamma_E - 5/2} t}{c_3 \langle \tau_B \rangle}\right) \right], \tag{61}$$

to be compared with Eq. (41). Employing the same considerations as in the CTRW case leads to the Laplace transform

$$\tilde{\psi}_B(\lambda) \approx 1 - \langle \tau_B \rangle \lambda - c_1 (\langle \tau_B \rangle \lambda)^2 \ln(\langle \tau_B \rangle \lambda), \tag{62}$$

which should be compared with Eq. (43). Again, the factor inside the logarithm cannot be determined exactly without knowledge of the full Eulerian PDF, but it does not impact the asymptotic behavior. Proceeding as before, we obtain

$$\sigma^2(t) \approx \frac{2c_1 \ell_c \langle V_E \rangle}{\chi^2} t \, \ln\left(\frac{\langle V_E \rangle t}{\ell_c}\right). \tag{63}$$

Comparing to Eq. (44), we find that late-time equivalence is again achieved by setting $\ell_d = 2\ell_c$. As before, we conclude that the $t \ln t$ dispersion scaling for Eulerian PDFs behaving as $\sim v^0$ near the origin is robust. The exponential PDF case, Eq. (60), is recovered upon setting $c_1 = 1$, up to the factor inside the logarithm.

Finally, consider a Eulerian PDF according to Eq. (45), corresponding to logarithmic corrections to $\sim v^{-1}$ behavior near the origin. The late-time behavior of the transit-time PDF is again dominated by the small-v behavior of the Eulerian PDF. Similarly to the CTRW model (see Appendix B), in order to determine the tailing behavior, the velocity integral in Eq. (55) can be performed up to an arbitrary cutoff,

$$\psi_B(t) \approx \frac{c_\alpha}{\ell_c \langle V_E \rangle} \int_0^{v_c/a} dv \, v \ln^{-1-\alpha}\left(\frac{v_c}{v}\right) e^{-vt/\ell_c}, \tag{64}$$

where $a > 1$ is a dimensionless constant and the cutoff ensures convergence. Performing the substitution $u = \ell_c/(vt)$ and rearranging terms, we obtain

$$\psi_B(t) \approx t^{-2} \ln^{-1-\alpha}\left(\frac{t}{t_c}\right) \int_{at_c/t}^\infty du \, u^{-3} \left(1 + \frac{\ln u}{\ln(ut/t_c)}\right)^{-1-\alpha} e^{-1/u}. \tag{65}$$

To leading order in large $t \gg t_c$, the remaining integral is given by $\int_0^\infty du \, u^{-3} e^{-1/u} = 1$, and we conclude that

$$\psi_B(t) \approx c_\alpha \langle \tau_B \rangle t^{-2} \ln^{-1-\alpha}(t/t_c). \tag{66}$$

Note that this result is independent of the arbitrary coefficient a as expected, and that it is identical to the CTRW transit-time PDF when $\ell_c = \ell_d$ [see Eq. (46)]. Proceeding as before, we find

$$\sigma^2(t) \approx \frac{c_\alpha \langle V_E \rangle^2}{\chi^2} t^2 \ln^{-1-\alpha}\left(\frac{v_c t}{\ell_c}\right). \tag{67}$$

Note again the independence of the prefactor on ℓ_c. Correspondingly, in this case, the Bernoulli and CTRW models are asymptotically equivalent regarding dispersion for any choice of ℓ_d and ℓ_c [see Eq. (48)]. Note that, as for the previous case and the CTRW, the exact factor inside the logarithm,
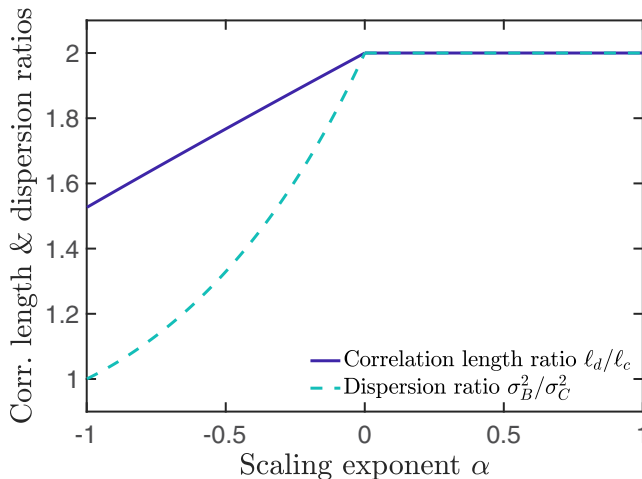
FIG. 1. Behavior of asymptotic dispersion in the Bernoulli relaxation model vs the CTRW, as a function of the scaling exponent α such that the Eulerian PDF $p_E(v) \sim v^\alpha$ at low velocities. Solid line: ratio of the CTRW decorrelation length ℓ_d to the Bernoulli relaxation model correlation length ℓ_c in order for asymptotic dispersion to be identical. Dashed line: ratio of asymptotic dispersion σ_B^2 in the Bernoulli model to dispersion σ_C^2 in the CTRW model when $\ell_d = \ell_c$.

which is irrelevant at sufficiently late times, cannot be determined without knowledge of the full Eulerian PDF.

C. Overview of results

We now present an overview of the results derived so far. We first collect our results for asymptotic dispersion, for different Eulerian PDFs and for both CTRW and Bernoulli relaxation models, in Table I. In addition, the solid line in Fig. 1 shows the ratio of the CTRW decorrelation length ℓ_d to correlation length ℓ_c of the Bernoulli relaxation model for equal asymptotic dispersion, as a function of the exponent α for a low-velocity Eulerian PDF dependency $\sim v^\alpha$ [see Eqs. (54) and (58)]. Note that this dependency is continuous at $\alpha = 0$. The dashed line in Fig. 1 shows the ratio between the asymptotic dispersion of the two models when $\ell_d = \ell_c$. For the logarithmically corrected $\sim v^{-1}$ Eulerian PDF analyzed here, we have seen that dispersion becomes independent of the correlation and decorrelation lengths [Eqs. (48) and (67)] and is equal in the two models. In this sense, the latter dependency is also right continuous at $\alpha = -1$. Recall that the results obtained here are valid for a flux-weighted initial condition. Although the scaling forms do not depend on the initial condition, the leading coefficients may [36].

Regarding our results for quasiballistic behavior, Eqs. (48) and (67), we note that similar log-corrected ballistic scalings were derived in [49], based on a CTRW model with a prescribed velocity PDF and step-size distribution accounting for velocity correlations. However, the choice of velocity distribution in that work is associated with an infinite mean transit time $\langle \tau \rangle$. This means that it cannot arise from a well defined $p_E(v)$ in the type of model we consider here [see Eqs. (10), (15), and related discussion].

IV. NUMERICAL SIMULATIONS

We now turn to numerical verification of the results for dispersion presented in Sec. III. Longitudinal positions and corresponding times are computed according to the recursion relations (7) for the CTRW and (12) for the spatial-Markov model with Bernoulli relaxation, with velocities in subsequent steps generated stochastically according to the prescriptions discussed in connection

with each model. Dispersion is computed from interpolated particle positions according to Eqs. (6) and (17). We set the decorrelation length of the CTRW and the correlation length of the Bernoulli model to $\ell_d = \ell_c = 1$ and tortuosity $\chi = 1$, which is equivalent to normalizing longitudinal distances by the longitudinal correlation length ℓ_c/χ, and correspondingly dispersion by ℓ_c^2/χ^2. For the Bernoulli model, we use a spatial step $\Delta s = 10^{-1}$. All simulation results are averaged over 10^5 particle trajectories.

A. Gamma-distributed Eulerian velocities

As an example of power-law dependency of the Eulerian PDF for small velocities, we employ a gamma PDF. Expressed in terms of the mean velocity and the usual scaling exponent $\gamma > 0$, such that $p_E(v) \propto v^{\gamma-1}$ at low velocities, this PDF is given by

$$p_E(v) = \frac{\gamma^\gamma}{\langle V_E \rangle \Gamma(\gamma)} \left(\frac{v}{\langle V_E \rangle} \right)^{\gamma-1} e^{-\gamma v/\langle V_E \rangle}. \tag{68}$$

The gamma PDF has been previously studied in connection with flow in porous media [15,20,36,50]. It provides a convenient model exhibiting two common features, namely, a power-law behavior at low velocities and an exponential tailing at high velocities. We note here that the assumption of power-law behavior near the origin is appropriate for most cases of interest: as the PDF is Taylor expanded around the origin, some power v (sometimes a constant, $\sim v^0$), typically dominates. Physically, this means that, below all relevant characteristic velocity scales, the low-velocity behavior is usually scale free (power law). Indeed, this type of behavior has been directly observed both numerically and experimentally [16,43,51–53]. An exception is the presence of logarithmic corrections which sometimes arise near a qualitative change of behavior; related examples are treated in Sec. IV B. According to Eq. (31), for a Eulerian PDF scaling as $\sim v^\alpha$ near the origin, we have

$$\alpha = \gamma - 1, \qquad c_\alpha = \frac{(1+\alpha)^{1+\alpha}}{\Gamma(1+\alpha)}. \tag{69}$$

For all $\alpha > -1$ (corresponding to $\gamma > 0$, which is required for normalizability of the PDF), direct calculation of the relevant moments according to Eq. (19) yields

$$\sigma_{V_0}^2 = \frac{2+\alpha}{(1+\alpha)^2} \langle V_E \rangle^2 \tag{70}$$

for the variance of the flux-weighted initial velocity distribution. Furthermore, from the definition of the average and Eq. (68), we find, for $\alpha > 0$ ($\gamma > 1$),

$$\langle V_E^{-1} \rangle = \frac{1+\alpha}{\alpha} \langle V_E \rangle^{-1}. \tag{71}$$

Thus, for $\alpha > 0$ ($\gamma > 1$), the second moment of the transit-time PDF is finite [see Eq. (11) for the CTRW and Eq. (16) for the Bernoulli model], and asymptotic dispersion is Fickian. For $\alpha < 0$ ($\gamma < 1$), the second moment diverges and asymptotic dispersion is superdiffusive. For $\alpha = 0$ ($\gamma = 1$), the gamma PDF reduces to the exponential PDF (35), which corresponds to superdiffusive but quasi-Fickian asymptotic dispersion.

Note that, according to Eqs. (3) and (68), the flux-weighted Eulerian PDF is again gamma, characterized by a mean $(2+\alpha)\langle V_E \rangle/(1+\alpha)$ and a power-law exponent $1+\alpha$. Thus, in this case, numerical simulations of the stochastic velocity process of Eqs. (7) and (12), which involve generating velocities according to the flux-weighted Eulerian PDF, were carried out by directly generating gamma-distributed values, without need for discretizing the underlying PDF. Figure 2 shows dispersion as a function of time for the cases $\alpha = -\frac{1}{2}$ [Fig. 2(a)], $\alpha = 0$ [Fig. 2(b)], and $\alpha = \frac{1}{2}$ [Fig. 2(c)]. These three cases correspond, respectively, to power-law non-Fickian dispersion, the exponential PDF case leading to quasi-Fickian dispersion, and Fickian dispersion (see Table I for the
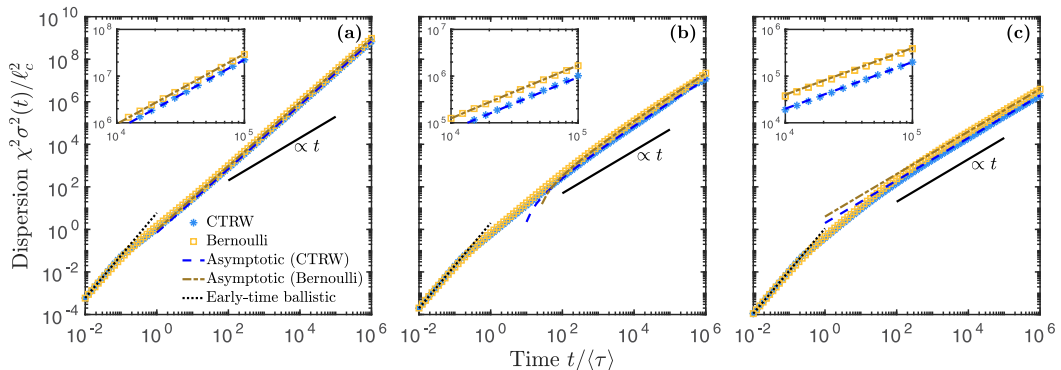
FIG. 2. Normalized dispersion $\chi^2 \sigma^2(t)/\ell_c^2$ versus normalized time $t/\langle\tau\rangle$ for gamma Eulerian velocity PDFs [Eq. (68)] which scale as $p_E(v) \sim v^\alpha$ near the origin, for a Bernoulli model with correlation length ℓ_c and a CTRW model with decorrelation length $\ell_d = \ell_c$. (a) $\alpha = -\frac{1}{2}$, corresponding to non-Fickian power-law asymptotic dispersion; (b) $\alpha = 0$, corresponding to quasi-Fickian asymptotic dispersion with logarithmic corrections; and (c) $\alpha = 1.5$, corresponding to Fickian asymptotic dispersion. Numerical simulation results for dispersion are shown as markers for the CTRW (squares) and Bernoulli (asterisks) models. The theoretical asymptotic forms of dispersion are shown as dashed lines for the CTRW and as dash-dotted lines for the Bernoulli model (see Table I for relevant equations). The insets show a zoom-in of part of the asymptotic region in the main plots. The scaling $\sigma^2(t) \propto t$ characteristic of Fickian dispersion is shown for reference as a solid line. Theoretical early-time ballistic dispersion [$\sigma^2(t) \propto t^2$, Eqs. (18) and (70)] is shown as dotted lines.

relevant equations). Times are normalized by the mean transit time $\langle\tau\rangle = \ell_c/\langle V_E\rangle = \ell_d/\langle V_E\rangle$, which is conveniently achieved by taking $\langle V_E\rangle = 1$ in the numerical simulations, along with $\ell_c = \ell_d = 1$ as discussed above. In all cases, the theoretical predictions for both the early-time ballistic regime and the asymptotic behavior of dispersion are in excellent agreement with the simulations.

B. Transition from quasi-Fickian to quasiballistic asymptotic dispersion in unsaturated porous media

Next, we turn to the two types of Eulerian PDF identified in [43], respectively, for saturated and unsaturated flow through two-dimensional porous media. In the original study, a sharp transition from quasi-Fickian to quasiballistic dispersion upon desaturation was identified through numerical simulations based on a CTRW model. This work provides a rigorous derivation of the associated dispersion scalings, and extends the CTRW results to the case of a correlated Bernoulli model. We briefly review the relevant aspects of the theory leading to the Eulerian PDFs studied here in Appendix D.

Under fully saturated conditions, we have the Eulerian PDF

$$p_E(v) = \frac{\sqrt{\pi}}{3v_c} \frac{2v}{3v_c} G_{12}^{20}\left(\frac{2v}{3v_c} \middle| \begin{matrix} -\frac{1}{2} \\ : -1, 0 \end{matrix}\right), \tag{72}$$

where G is the Meijer G function [54] and $v_c = q_c/a_m$ is a characteristic velocity. Direct computation of the mean value using the properties of the Meijer G function yields $\langle V_E\rangle = 2v_c$, and calculation of the relevant higher-order moments leads, according to Eq. (19), to

$$\sigma_{V_0}^2 = \frac{972}{175}v_c^2 = \frac{243}{175}\langle V_E\rangle^2. \tag{73}$$

For small velocities $v \ll v_c$, Eq. (41) holds, with [43]

$$c_1 = c_2 = \frac{2}{3}, \qquad c_3 = \frac{4}{3}\exp[F(-1/2) - 2(1 - \gamma_E)], \tag{74}$$

where F is the digamma function, $F(x) = d \ln\Gamma(x)/dx$ [in particular, $F(1) = -\gamma_E$].
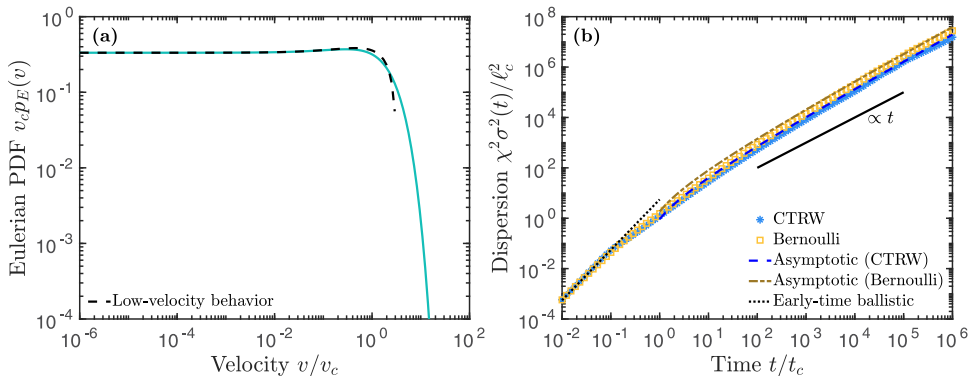
FIG. 3. (a) Eulerian velocity PDF $v_c p_E(v)$ [Eq. (72)] for fully saturated conditions, as discussed in Appendix D, and (b) corresponding normalized dispersion $\chi^2 \sigma^2(t)/\ell_c^2$ versus normalized time t/t_c for a Bernoulli model with correlation length ℓ_c and a CTRW model with decorrelation length $\ell_d = \ell_c$. The low-velocity behavior of the PDF, shown by the dashed line in (a), is given by Eq. (40) with coefficients given by Eq. (74). Numerical simulation results for dispersion are shown as markers for the CTRW (squares) and Bernoulli (asterisks) models. Dispersion is asymptotically quasi-Fickian with logarithmic corrections. The theoretical asymptotic forms of dispersion are shown as dashed lines for the CTRW and as dash-dotted lines for the Bernoulli model (see Table I for relevant equations). The scaling $\sigma^2(t) \propto t$ characteristic of Fickian dispersion is shown for reference as a solid line. Theoretical early-time ballistic dispersion [$\sigma^2(t) \propto t^2$, Eqs. (18) and (73)].

In this case, no analytical transform is available to generate velocities according to the flux-weighted Eulerian PDF from uniformly distributed samples. We thus compute the Eulerian PDF according to Eq. (72) for 300 logarithmically spaced values of velocity from $v = 10^{-15} v_c$ to $10^2 v_c$. These values are employed as the edges of discretized velocity bins. Bin flux-weighted probabilities are obtained according to Eq. (3), using the midpoint values of velocity and the Eulerian PDF and multiplying by the corresponding bin width. Velocity values are then generated based on the resulting discretized probability distribution. The Eulerian PDF (72) and the associated dispersion under the CTRW and Bernoulli models are shown in Fig. 3. In this case, we normalize velocities by the characteristic velocity v_c by setting $v_c = 1$, which, for $\ell_c = \ell_d = 1$, is equivalent to normalizing times by the characteristic time $t_c = \ell_c/v_c$. The simulations are in agreement with the theoretical predictions for both the early-time ballistic and asymptotic quasi-Fickian regimes.

Under unsaturated conditions, the full PDF must be computed numerically, but its low- and high-velocity dependencies were obtained in [43]. In particular, the low-velocity dependency, for $v \ll v_c$, is given by Eq. (45) with α related to the distribution of dead-end regions (see Appendix D), and

$$c_\alpha = \frac{\alpha f}{1 + \alpha}, \tag{75}$$

where f is the fraction of the domain occupied by dead-end regions. We employ the same velocity PDF discretization procedure as for the fully saturated case in order to generate flux-weighted velocity values in the numerical simulations. The Eulerian mean velocity, as well as higher-order moments relevant for early-time dispersion [Eqs. (18) and (19)], were computed numerically from the discretized PDF. As a representative example, we take $f = 0.12$ and $\alpha = 0.5$, which were found in [43] for a water saturation of 77%. Note that the qualitative behavior is independent of saturation, as long as the medium is not fully saturated. The full numerically computed Eulerian PDF and the corresponding dispersion under the CTRW and Bernoulli models are shown, respectively, in Figs. 3(a) and 3(b). We again normalize velocities by v_c by setting $v_c = 1$ and times by the characteristic time $t_c = \ell_c/v_c$. We find agreement between the expected early-time ballistic and

asymptotic quasiballistic behavior and the numerical simulations (see Table I for the relevant equations). Note how the very broad nature of the Eulerian PDF leads in this case to a late onset of the true asymptotic regime. In [43], due to the finite size of the medium, only the preasymptotic regime, seen here in the range of times $t_c \lesssim t \lesssim 10^4 t_c$, was observed. This intermediate regime is found here to be well approximated by power-law growth in time with an exponent ≈ 1.4. This behavior is superdiffusive and markedly more anomalous than the saturated case, for which dispersion scales as $t \ln t$. Notwithstanding, the true asymptotic regime again exhibits significantly faster dispersion growth, characterized by a quasiballistic scaling $\sim t^2 \ln^{-1-\alpha} t$.

V. CONCLUSIONS

We have provided a detailed comparison of a correlated and an uncorrelated space-Lagrangian model regarding dispersion. In particular, we have extended previous results for the equivalence of asymptotic temporal scaling forms to Eulerian PDFs exhibiting logarithmically corrected scalings at low velocities. However, we have found that full asymptotic equivalence of the two models does not hold in general when the CTRW step length is taken equal to the longitudinal velocity correlation length.

As we have seen, for equal correlation lengths, dispersion in the Bernoulli model is generally larger than in the CTRW model. This happens because the differences in correlation structure lead to stronger correlations in the velocity fluctuations in the Bernoulli model. The two models can be rendered equivalent by choosing a larger (de)correlation length for the CTRW model, but the relation between these lengths depends on the low-velocity characteristics of the Eulerian PDF, which control the properties of asymptotic dispersion (see Fig. 1). Nonetheless, the functional form of the asymptotic temporal scaling in both models is the same in all cases, regardless of (de)correlation length. In particular, this means that a CTRW model is typically sufficient to capture asymptotic dispersion, but the correct choice of step length will generally not match the physical correlation length of Lagrangian velocities.

We have obtained results for dispersion for the qualitatively different Eulerian PDFs found in [43] for saturated and unsaturated (quasi-)two-dimensional porous media (see Figs. 3 and 4). Our results provide a rigorous theoretical basis for the sharp transition from quasi-Fickian to quasiballistic dispersion which was observed in [43] upon desaturation. In particular, our results show that the quasiballistic behavior associated with the Eulerian PDFs under unsaturated conditions is robust and insensitive to the presence of nontrivial velocity correlations.

ACKNOWLEDGMENTS

APPENDIX A: VARIANCE OF THE NUMBER OF CTRW STEPS

In this Appendix, we obtain the Laplace transform of the variance of the number of CTRW steps, in terms of the transit-time PDF associated with each step. First, note that the probability of completing exactly n steps by time t is equal to the probability of completing at least n steps, minus the probability of completing at least $n + 1$ steps [55],

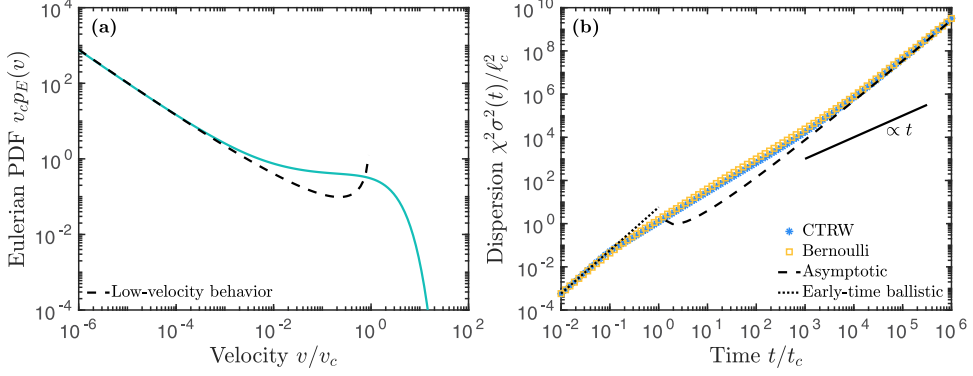$$p_n(t) = P[N(t) \geqslant n] - P[N(t) \geqslant n + 1]. \tag{A1}$$

FIG. 4. (a) Eulerian velocity PDF $v_c p_E(v)$ obtained for unsaturated conditions as discussed in Appendix D, and (b) corresponding normalized dispersion $\chi^2 \sigma^2(t)/\ell_c^2$ versus normalized time t/t_c for a Bernoulli model with correlation length ℓ_c and a CTRW model with decorrelation length $\ell_d = \ell_c$. The low-velocity behavior of the PDF, shown as a dashed line in (a), is given by Eq. (45) with c_α according to Eq. (75) for $f = 0.12$ and $\alpha = 0.5$. Numerical simulation results for dispersion are shown as markers for the CTRW (squares) and Bernoulli (asterisks) models. Dispersion is asymptotically quasiballistic with logarithmic corrections. The theoretical asymptotic forms of dispersion for the CTRW and Bernoulli models are identical and shown as a dashed line (see Table I for relevant equations). The scaling $\sigma^2(t) \propto t$ characteristic of Fickian dispersion is shown for reference as a solid line. Theoretical early-time ballistic dispersion [$\sigma^2(t) \propto t^2$, Eqs. (18) and (19)] is shown as a dash-dotted line.

The probability of completing at least n steps by time t is, by definition, the probability that the time of completing the nth step $T_n \leqslant t$. Since

$$T_n = \sum_{i=0}^{n-1} \tau_i \tag{A2}$$

is the sum of n independently and identically distributed random variables, its PDF is the n-fold convolution of ψ with itself, which we denote by ψ^{*n}. Thus,

$$P[N(t) \geqslant n] = \int_0^t dt' \psi^{*n}(t'). \tag{A3}$$

This leads, Laplace transforming Eq. (A1), to

$$\tilde{p}_n(\lambda) = \frac{1 - \tilde{\psi}(\lambda)}{\lambda} \tilde{\psi}^n(\lambda). \tag{A4}$$

We first compute the mean number of transitions by time t,

$$\langle N(t) \rangle = \sum_{n \geqslant 0} n p_n(t). \tag{A5}$$

Taking Laplace transforms,

$$\langle \tilde{N}(\lambda) \rangle = \frac{1 - \tilde{\psi}(\lambda)}{\lambda} \sum_{n \geqslant 0} n \tilde{\psi}^n(\lambda) = \frac{1 - \tilde{\psi}(\lambda)}{\lambda} \tilde{\psi}(\lambda) \frac{d}{d\tilde{\psi}(\lambda)} \sum_{n \geqslant 0} \tilde{\psi}^n(\lambda) = \frac{1 - \tilde{\psi}(\lambda)}{\lambda} \tilde{\psi}(\lambda)$$

$$\times \frac{d}{d\tilde{\psi}(\lambda)} \frac{1}{1 - \tilde{\psi}(\lambda)}, \tag{A6}$$

which yields Eq. (22a). Similarly, for the second moment, we have

$$\langle \widetilde{N^2}(\lambda) \rangle = \frac{1 - \tilde{\psi}(\lambda)}{\lambda} \sum_{n \geqslant 0} n^2 \tilde{\psi}^n(\lambda) = \frac{1 - \tilde{\psi}(\lambda)}{\lambda}$$

$$\times \left[\tilde{\psi}(\lambda)^2 \frac{d^2}{d\tilde{\psi}(\lambda)^2} \sum_{n \geqslant 0} \tilde{\psi}^n(\lambda) + \tilde{\psi}(\lambda) \frac{d}{d\tilde{\psi}(\lambda)} \sum_{n \geqslant 0} \tilde{\psi}^n(\lambda) \right], \qquad (A7)$$

yielding Eq. (22b).

APPENDIX B: SOME LAPLACE TRANSFORMS INVOLVING POWERS OF LOGARITHMS

Here, we obtain some results for Laplace transforms involving powers of logarithms. We then employ these results to compute the first and second moments of the number of steps in the quasiballistic CTRW model of Sec. III A 2 of the main text; the mean and second moments of position in the corresponding Bernoulli model of Sec. III B 2 can be computed in a similar manner, as also discussed in the main text. Consider a transit-time PDF with finite mean $\langle \tau \rangle$ and such that, for t large compared to some characteristic value t_d, we have the tailing behavior

$$\psi(t) \approx c_\alpha \langle \tau \rangle t^{-2} \ln(t/t_d)^{-1-\alpha}, \qquad (B1)$$

for some dimensionless $c_\alpha > 0$ and $\alpha > 0$. Since ψ is normalized to unit integral by definition, we have $\tilde{\psi}(0) = 1$. Since its mean is finite by hypothesis, we have also $d\tilde{\psi}(\lambda)/d\lambda|_{\lambda=0} = -\langle \tau \rangle$. We seek the next leading term in the small-λ behavior of $\tilde{\psi}(\lambda)$, which we know must be of higher order than λ^2 because second moments associated with this tailing behavior diverge.

The effect of the tailing behavior on the Laplace PDF can be obtained by computing the Laplace transform of the tail

$$\tilde{L}(\lambda) = c_\alpha \langle \tau \rangle \int_{at_d}^{\infty} dt\, t^{-2} \ln^{-1-\alpha}(t/t_d) e^{-\lambda t}, \qquad (B2)$$

with a dimensionless $a > 1$ to guarantee the integral converges. Note that, for smaller times, the early-time behavior of $\psi(t)$ plays a role, but this does not contribute to the tailing behavior. Indeed, as will be confirmed below, the result is independent of the arbitrary coefficient a. Integrating by parts once (differentiating the exponential) gives

$$\tilde{L}(\lambda) = \frac{c_\alpha \langle \tau \rangle \lambda}{t_d} \int_{at_d}^{\infty} dt\, (\Gamma(-\alpha, \ln a) - \Gamma[-\alpha, \ln(t/t_d)]) e^{-\lambda t}, \qquad (B3)$$

where $\Gamma(\cdot, \cdot)$ is the upper incomplete gamma function, $\Gamma(a, z) = \int_z^{\infty} dx\, x^{a-1} e^{-x}$. Integrating once more by parts and approximating for small $\lambda \ll 1/t_d$,

$$\tilde{L}(\lambda) \approx \frac{c_\alpha \langle \tau \rangle}{t_d} \left[\Gamma(-\alpha, \ln a) - \frac{t_d \lambda}{\alpha} \ln^{-\alpha} a \right] e^{-at_d \lambda} + \frac{c_\alpha \langle \tau \rangle \lambda^2}{\alpha} [\tilde{J}_\alpha(\lambda) - \alpha \tilde{J}_{1+\alpha}(\lambda)], \qquad (B4)$$

where, for any real β,

$$\tilde{J}_\beta(\lambda) = \int_{at_d}^{\infty} dt\, \ln^{-\beta}(t/t_d) e^{-\lambda t} \qquad (B5)$$

is the Laplace transform of a tail $J_\beta(t) = \ln^{-\beta}(t/t_d), t \geqslant at_d$.

The first term in Eq. (B4) has a regular expansion in non-negative powers of small $\lambda \ll 1/t_d$. These expansion terms do not correspond to the correct normalization condition and mean of ψ, due to the missing integration up to $t = at_d$. We can simply restore these contributions to obtain

$$\tilde{\psi}(\lambda) \approx 1 - \langle \tau \rangle \lambda + \frac{c_\alpha \langle \tau \rangle \lambda^2}{\alpha} [\tilde{J}_\alpha(\lambda) - \alpha \tilde{J}_{1+\alpha}(\lambda)]. \qquad (B6)$$

It remains to calculate $\tilde{J}_\beta(\lambda)$ to leading order, which will be seen to be of negative order in λ. To this end, we employ the substitution $u = \lambda t$ in Eq. (B5). Rearranging terms,

$$\tilde{J}_\beta(\lambda) = \lambda^{-1} \ln^{-\beta} \left(\frac{1}{t_d \lambda} \right) \int_{at_d \lambda}^{\infty} du \left[1 + \frac{\ln u}{\ln[1/(t_d \lambda)]} \right]^{-\beta} e^{-u}. \tag{B7}$$

For $\lambda < 1/(at_d)$, the integral can be split as $\int_{at_d\lambda}^{\infty} = \int_{at_d\lambda}^{1/(t_d\lambda)} + \int_{1/(t_d\lambda)}^{\infty}$. The second contribution can be bounded from above by setting $u = a$ in the integrand, and the result vanishes exponentially in $1/\lambda$. For the first contribution, expanding the term in square brackets for small λ, the integrals of the expansion terms all converge, and we find to leading order

$$\tilde{J}_\beta(\lambda) \approx \lambda^{-1} \ln^{-\beta} \left(\frac{1}{t_d \lambda} \right) \left[1 + \alpha \gamma_E \ln^{-1} \left(\frac{1}{t_d \lambda} \right) \right]. \tag{B8}$$

We note that, since it is independent of a, this result is also the small-λ expansion of the Laplace transform of any function integrable near the origin and tailing as $J_\beta(t) = \ln^{-\beta}(t/t_d)$ for large t [see Eq. (B5)]. We thus finally arrive at the desired result (47), which is independent of the arbitrary coefficient a as expected.

This derivation allows us to obtain two related inverse Laplace transforms which are needed to compute dispersion. Recall that division by λ in Laplace space corresponds to integration in the time domain. Writing $\mathcal{L}_{\lambda \to t}^{-1} \tilde{f}(\lambda) = f(t)$, we find the inverse Laplace transforms

$$\mathcal{L}_{\lambda \to t}^{-1} \lambda^{-1} \tilde{J}_\beta(\lambda) = \int_{at_d}^{t} du \, \ln^{-\beta} \left(\frac{u}{t_d} \right) \approx -t_d \ln^{1-\beta} \left(\frac{t}{t_d} \right) E_\beta \left[-\ln \left(\frac{t}{t_d} \right) \right],$$

$$\approx t \, \ln^{-\beta} \left(\frac{1}{t_d \lambda} \right) \left[1 + \beta \, \ln^{-1} \left(\frac{1}{t_d \lambda} \right) \right], \tag{B9}$$

where $E_\beta(z) = \int_1^\infty dx \, x^{-\alpha} \exp(-zx)$ is an exponential integral. Proceeding similarly, one further time integration yields

$$\mathcal{L}_{\lambda \to t}^{-1} \lambda^{-2} \tilde{J}_\beta(\lambda) \quad \approx -t_d^2 \ln^{-1-\beta} \left(\frac{t}{t_d} \right) E_\beta \left[-2 \ln \left(\frac{t}{t_d} \right) \right]$$

$$\approx \frac{t^2}{2} \ln^{-\beta} \left(\frac{1}{t_d \lambda} \right) \left[1 + \frac{3\beta}{2} \ln^{-1} \left(\frac{1}{t_d \lambda} \right) \right]. \tag{B10}$$

Equations (B9) and (B10) are valid for small $\lambda \ll 1/t_d$ and large $t \gg t_d$, and again independent of a as expected.

We now apply these results to compute the first and second moments of the number of steps in a CTRW with a transit-time PDF tailing according to Eq. (B1). Substituting Eq. (B6) for the Laplace transform of the transit time for small $\lambda \ll 1/t_d$ in Eq. (22a), we obtain to leading order

$$\langle \tilde{N}(\lambda) \rangle \approx (\langle \tau \rangle \lambda)^{-1} \left[1 + \frac{c_\alpha}{\alpha} [J_\alpha(\lambda) - \alpha J_{1+\alpha}(\lambda)] + \frac{c_\alpha^2}{\alpha^2} J_{2\alpha}(\lambda) \right], \tag{B11}$$

where we have used Eq. (B8) to conclude that $[\tilde{J}_\alpha(\lambda) - \alpha \tilde{J}_{1+\alpha}(\lambda)]^2 \approx \tilde{J}_{2\alpha}$ to leading order. Using Eq. (B9), we obtain, for $t \gg t_d$,

$$\langle N(t) \rangle \approx \frac{t}{\langle \tau \rangle} \left[1 + \frac{c_\alpha}{\alpha} \ln^{-\alpha} \left(\frac{t}{t_d} \right) + \frac{c_\alpha^2}{\alpha^2} \ln^{-2\alpha} \left(\frac{t}{t_d} \right) \right]. \tag{B12}$$

For the second moment, we proceed similarly, according to Eq. (22b), and find

$$\langle \widetilde{N^2}(\lambda) \rangle \approx (\langle \tau \rangle \lambda)^{-2} \left[1 + \frac{2c_\alpha}{\alpha} [J_\alpha(\lambda) - \alpha J_{1+\alpha}(\lambda)] + \frac{3c_\alpha^2}{\alpha^2} J_{2\alpha}(\lambda) \right]. \tag{B13}$$

Using Eq. (B10) leads to

$$\langle N^2(t)\rangle \approx \frac{t^2}{\langle\tau\rangle^2}\left[1 + \frac{2c_\alpha}{\alpha}\ln^{-\alpha}\left(\frac{t}{t_d}\right) + \frac{c_\alpha}{\alpha}\ln^{-1-\alpha}\left(\frac{t}{t_d}\right) + \frac{3c_\alpha^2}{\alpha^2}\ln^{-2\alpha}\left(\frac{t}{t_d}\right)\right]. \tag{B14}$$

Using Eq. (21) together with $\langle\tau\rangle = \ell_d/\langle V_E\rangle$ [Eq. (8)], dispersion is given to leading order in large time by Eq. (48).

APPENDIX C: SINGLE- AND TWO-POINT MEAN VELOCITY IN THE BERNOULLI RELAXATION MODEL

Determining asymptotic dispersion in the Bernoulli model requires computing the time integrals $I_1(t)$ and $I_2(t)$ of the single- and two-point mean velocity, defined according to Eqs. (50). In order to do so, we make use of some results obtained in [36], focusing on the case of a flux-weighted initial condition. A similar calculation for the case of a spatially homogeneous initial condition (i.e., with velocities distributed according to p_E) can be found in [20]. According to [36], and particularizing for the case of a flux-weighted initial condition, the PDF $p_T(\cdot;t)$ of time-Lagrangian velocities $V_T(t)$, defined such that $p_T(v;t)\,dv$ is the probability that $V_T(t)$ is between v and $v + dv$, has a Laplace transform with respect to time given by

$$\tilde{p}_T(v;\lambda) = \frac{\ell_c p_E(v)}{\langle V_E\rangle[1 - \tilde{\psi}_B(\lambda)](1 + \ell_c\lambda/v)}. \tag{C1}$$

We have, by definition,

$$\langle V_T(t)\rangle = \int_0^\infty dv\, v p_T(v;t). \tag{C2}$$

Using these results along with Eqs. (50a) and (C1) leads directly to Eq. (51a).

The calculation of the two-point average is more involved because correlation between velocities at different times must be taken into account. For $t > t'$, conditioning on velocity v at time t', it is given by

$$\langle V_T(t)V_T(t')\rangle = \int_0^\infty dv\, \langle V_T(t-t')|v\rangle v p_T(v;t'), \tag{C3}$$

where $\langle V_T(t)|v\rangle$ is the average velocity at time t given velocity v at $t = 0$. Thus, using Eq. (50b),

$$\tilde{I}_2(\lambda) = \frac{2}{\ell_c^2\lambda}\int_0^\infty dv\, \langle\tilde{V}_T(\lambda)|v\rangle v\tilde{p}_T(v;\lambda). \tag{C4}$$

Rearranging the result found in [36], we have the Laplace transform

$$\langle\tilde{V}_T(\lambda)|v\rangle = \frac{1}{1 - \tilde{\psi}_B(\lambda)}\frac{\ell_c}{1 + \ell_c\lambda/v}, \tag{C5}$$

and we find

$$\tilde{I}_2(\lambda) = \frac{2}{\lambda[1 - \tilde{\psi}_B(\lambda)]^2}\int_0^\infty dv\, \frac{p_F(v)}{(1 + \ell_c\lambda/v)^2}. \tag{C6}$$

Using Eq. (14) leads to Eq. (51b) to leading in small $\lambda \ll 1/\langle\tau_B\rangle$.

APPENDIX D: VELOCITY PDFS UNDER SATURATED AND UNSATURATED CONDITIONS IN QUASI-2D POROUS MEDIA

We briefly review the relevant aspects of the theory leading to the Eulerian PDFs studied here. In the original study, the authors considered a quasi-two-dimensional (2D) porous medium filled with water and air at different water saturation degrees (i.e., percentage of the pore space occupied by

water) [56]. The capillary number was sufficiently low to ensure air clusters remained immobile. The authors developed a theoretical model for the corresponding Eulerian velocity PDFs characterizing the flow of water, accounting for drag effects along the third dimension (thickness) of quasi-two-dimensional media. Here, we focus for simplicity on the purely two-dimensional limit (also studied in the original paper), but we note that the asymptotic scaling forms of dispersion remain unaffected by the three-dimensional corrections.

In the model of [43], the Eulerian PDF is determined by the flow rate PDF $p_Q(q)$ of total flow rates q across pore throats (i.e., smallest distance between two neighboring grains) throughout the domain, weighted by the PDF $p_E(v|q)$ of velocities v within a pore with given flow rate q:

$$p_E(v) = \int_0^\infty dq \, p_Q(q) p_E(v|q). \tag{D1}$$

Given the low variability of pore-throat sizes across the medium, the throat size was approximated by the average value a_m. Considering a purely two-dimensional medium, the Eulerian velocity PDF associated with the velocity profile across a pore throat with local flow rate q is then the PDF of a Poiseuille flow (see also [20]),

$$p_E(v|q) = \frac{a_m H[3q/(2a_m) - v]}{3q\sqrt{1 - 2a_m v/(3q)}}, \tag{D2}$$

where H is the Heaviside step function. The flow PDFs p_Q were obtained based on a decomposition of the water phase into a backbone of high velocities and dead ends of low velocities, caused by the presence of the air phase (see also [57]):

$$p_Q(q) = f p_Q^d(q) + (1 - f) p_Q^b(q), \tag{D3}$$

where f is the fraction of the domain occupied by dead-end regions, $p_Q^d(q)$ is the PDF of flow rates within the latter, and p_Q^b is the PDF of flow rates in the backbone. The backbone contribution is described by a gamma distribution (see also [50])

$$p_Q^b(q) = \frac{q e^{-q/q_c}}{q_c^2}, \tag{D4}$$

where q_c is a saturation-dependent characteristic flow rate which controls the exponential high-flow tailing.

Under fully saturated conditions, $f = 0$, and the full flow rate PDF p_Q coincides with p_Q^b. In that case, Eq. (D1) leads to the Eulerian PDF (72). Under unsaturated conditions, the dead-end contribution to the flow PDF is given by [43]

$$p_Q^d(q) \approx \int_0^\infty dA \, p_Q^d(q|\sqrt{A}) p_A(A), \tag{D5}$$

where

$$p_Q^d(q|\ell) = \frac{a_m}{\ell q_c q} \left[e^{-q/q_c}(q + q_c) - \exp\left(-\frac{e^{\ell/a_m} q}{q_c}\right)(e^{\ell/a_m} q + q_c) \right] \tag{D6}$$

is the flow rate PDF for a dead-end region of given depth ℓ, and the dead-end area PDF p_A follows a Pareto distribution

$$p_A(A) = \frac{\gamma}{a_m^2} \left(\frac{A}{a_m^2}\right)^{-1-\gamma} H(A - a_m^2). \tag{D7}$$

The exponent γ decreases with decreasing water saturation, reflecting broader dead-end area variability. The full flow rate PDF p_Q is then obtained by substituting Eqs. (D4) and (D5) in Eq. (D3), and the corresponding Eulerian velocity PDF is determined by Eq. (D1). While the full PDF must be

computed numerically, its low- and high-velocity dependencies were obtained in [43]. In particular, the low-velocity dependency, for $v \ll v_c$, is given by Eq. (45) with $\alpha = 2\gamma$ and $c_\alpha = f\alpha/(1 + \alpha)$.

[1] B. Berkowitz, A. Cortis, M. Dentz, and H. Scher, Modeling non-Fickian transport in geological formations as a continuous time random walk, Rev. Geophys. **44**, RG2003 (2006).

[2] R. Klages, G. Radons, and I. M. Sokolov, *Anomalous Transport: Foundations and Applications* (Wiley, Hoboken, NJ, 2008).

[3] R. Metzler and J. Klafter, The restaurant at the end of the random walk: recent developments in the description of anomalous transport by fractional dynamics, J. Phys. A: Math. Gen. **37**, R161 (2004).

[4] S. B. Pope, Simple models of turbulent flows, Phys. Fluids **23**, 011301 (2011).

[5] N. Sund, T. Aquino, and D. Bolster, Effective models for transport in complex heterogeneous hydrologic systems, in *Encyclopedia of Water: Science, Technology, and Society*, edited by Patricia Maurice (Wiley, Hoboken, NJ, 2019).

[6] H. Scher and M. Lax, Stochastic transport in a disordered solid. I. Theory, Phys. Rev. B **7**, 4491 (1973).

[7] R. Metzler and J. Klafter, The random walk's guide to anomalous diffusion: a fractional dynamics approach, Phys. Rep. **339**, 1 (2000).

[8] T. Le Borgne, M. Dentz, and J. Carrera, Spatial Markov processes for modeling Lagrangian particle dynamics in heterogeneous porous media, Phys. Rev. E **78**, 026308 (2008).

[9] P. De Anna, T. Le Borgne, M. Dentz, A. M. Tartakovsky, D. Bolster, and P. Davy, Flow Intermittency, Dispersion, and Correlated Continuous Time Random Walks in Porous Media, Phys. Rev. Lett. **110**, 184502 (2013).

[10] T. Sherman, N. B. Engdahl, G. Porta, and D. Bolster, A review of spatial Markov models for predicting pre-asymptotic and anomalous transport in porous and fractured media, J. Contam. Hydrol. **236**, 103734 (2020).

[11] T. Le Borgne, M. Dentz, and J. Carrera, Lagrangian Statistical Model for Transport in Highly Heterogeneous Velocity Fields, Phys. Rev. Lett. **101**, 090601 (2008).

[12] D. W. Meyer and H. A. Tchelepi, Particle-based transport model with Markovian velocity processes for tracer dispersion in highly heterogeneous porous media, Water Resour. Res. **46**, W11552 (2010).

[13] D. W. Meyer and F. Saggini, Testing the Markov hypothesis in fluid flows, Phys. Rev. E **93**, 053103 (2016).

[14] P. K. Kang, P. De Anna, J. P. Nunes, B. Bijeljic, M. J. Blunt, and R. Juanes, Pore-scale intermittent velocity structure underpinning anomalous transport through 3-D porous media, Geophys. Res. Lett. **41**, 6184 (2014).

[15] M. Holzner, V. L. Morales, M. Willmann, and M. Dentz, Intermittent Lagrangian velocities and accelerations in three-dimensional porous medium flow, Phys. Rev. E **92**, 013015 (2015).

[16] A. Puyguiraud, P. Gouze, and M. Dentz, Stochastic dynamics of Lagrangian pore-scale velocities in three-dimensional porous media, Water Resour. Res. **55**, 1196 (2019).

[17] V. Hakoun, A. Comolli, and M. Dentz, Upscaling and prediction of Lagrangian velocity dynamics in heterogeneous porous media, Water Resour. Res. **55**, 3976 (2019).

[18] A. Comolli, V. Hakoun, and M. Dentz, Mechanisms, upscaling, and prediction of anomalous dispersion in heterogeneous porous media, Water Resour. Res. **55**, 8197 (2019).

[19] M. Dentz, A. Comolli, V. Hakoun, and J. J. Hidalgo, Transport upscaling in highly heterogeneous aquifers and the prediction of tracer dispersion at the made site, Geophys. Res. Lett. **47**, e2020GL088292 (2020).

[20] T. Aquino and T. Le Borgne, The diffusing-velocity random walk: a spatial-Markov formulation of heterogeneous advection and diffusion, J. Fluid Mech. **910**, A12 (2021).

[21] M. Dentz, A. Cortis, H. Scher, and B. Berkowitz, Time behavior of solute transport in heterogeneous media: transition from anomalous to normal transport, Adv. Water Resour. **27**, 155 (2004).

[22] B. Bijeljic and M. J. Blunt, Pore-scale modeling and continuous time random walk analysis of dispersion in porous media, Water Resour. Res. **42**, W01202 (2006).

[23] A. Puyguiraud, P. Gouze, and M. Dentz, Upscaling of anomalous pore-scale dispersion, Transp. Porous Media **128**, 837 (2019).

[24] A. Puyguiraud, P. Gouze, and M. Dentz, Pore-Scale Mixing and the Evolution of Hydrodynamic Dispersion in Porous Media, Phys. Rev. Lett. **126**, 164501 (2021).

[25] P. K. Kang, M. Dentz, T. Le Borgne, and R. Juanes, Spatial Markov Model of Anomalous Transport Through Random Lattice Networks, Phys. Rev. Lett. **107**, 180602 (2011).

[26] P. K. Kang, T. Le Borgne, M. Dentz, O. Bour, and R. Juanes, Impact of velocity correlation and distribution on transport in fractured media: Field evidence and theoretical model, Water Resour. Res. **51**, 940 (2015).

[27] P. K. Kang, M. Dentz, T. Le Borgne, S. Lee, and R. Juanes, Anomalous transport in disordered fracture networks: Spatial Markov model for dispersion with variable injection modes, Adv. Water Resour. **106**, 80 (2017).

[28] T. Sherman, A. Fakhari, S. Miller, K. Singha, and D. Bolster, Parameterizing the spatial Markov model from breakthrough curve data alone, Water Resour. Res. **53**, 10888 (2017).

[29] D. Bolster, Y. Méheust, T. Le Borgne, J. Bouquain, and P. Davy, Modeling preasymptotic transport in flows with significant inertial and trapping effects - the importance of velocity correlations and a spatial Markov model, Adv. Water Resour. **70**, 89 (2014).

[30] N. Sund, D. Bolster, S. Mattis, and C. Dawson, Pre-asymptotic transport upscaling in inertial and unsteady flows through porous media, Transp. Porous Media **109**, 411 (2015).

[31] J. S. Kim and P. K. Kang, Anomalous transport through free-flow-porous media interface: Pore-scale simulation and predictive modeling, Adv. Water Resour. **135**, 103467 (2020).

[32] N. L. Sund, G. M. Porta, and D. Bolster, Upscaling of dilution and mixing using a trajectory based spatial Markov random walk model in a periodic flow domain, Adv. Water Resour. **103**, 76 (2017).

[33] N. Sund, G. Porta, D. Bolster, and R. Parashar, A Lagrangian transport Eulerian reaction spatial (LATERS) Markov model for prediction of effective bimolecular reactive transport, Water Resour. Res. **53**, 9040 (2017).

[34] E. E. Wright, N. L. Sund, D. H. Richter, G. M. Porta, and D. Bolster, Upscaling mixing in highly heterogeneous porous media via a spatial Markov model, Water **11**, 53 (2019).

[35] T. Sherman, A. Paster, G. Porta, and D. Bolster, A spatial Markov model for upscaling transport of adsorbing-desorbing solutes, J. Contam. Hydrol. **222**, 31 (2019).

[36] M. Dentz, P. K. Kang, A. Comolli, T. Le Borgne, and D. R. Lester, Continuous time random walks for the evolution of Lagrangian velocities, Phys. Rev. Fluids **1**, 074004 (2016).

[37] H. Scher and E. W. Montroll, Anomalous transit-time dispersion in amorphous solids, Phys. Rev. B **12**, 2455 (1975).

[38] I. M. Sokolov, Models of anomalous diffusion in crowded environments, Soft Matter **8**, 9043 (2012).

[39] D. A. Benson and M. M. Meerschaert, A simple and efficient random walk solution of multi-rate mobile/immobile mass transport equations, Adv. Water Resour. **32**, 532 (2009).

[40] A. Comolli, J. J. Hidalgo, C. Moussey, and M. Dentz, Non-Fickian transport under heterogeneous advection and mobile-immobile mass transfer, Transp. Porous Media **115**, 265 (2016).

[41] M. F. Shlesinger, Asymptotic solutions of continuous-time random walks, J. Stat. Phys. **10**, 421 (1974).

[42] G. Margolin and B. Berkowitz, Spatial behavior of anomalous transport, Phys. Rev. E **65**, 031101 (2002).

[43] A. Velásquez-Parra, T. Aquino, M. Willmann, Y. Méheust, T. Le Borgne, and J. Jiménez-Martínez, Sharp transition to strongly anomalous transport in unsaturated porous media, Geophysical Research Letters **49**, e2021GL096280 (2022).

[44] A. Koponen, M. Kataja, and J. V. Timonen, Tortuous flow in porous media, Phys. Rev. E **54**, 406 (1996).

[45] B. Ghanbarian, A. G. Hunt, R. P. Ewing, and M. Sahimi, Tortuosity in porous media: a critical review, Soil Sci. Soc. Am. J. **77**, 1461 (2013).

[46] W. Feller, *An Introduction to Probability Theory and its Applications*, Volume 2 (Wiley, Hoboken, NJ, 2008).

[47] M. M. Meerschaert and A. Sikorskii, *Stochastic Models for Fractional Calculus*, Volume 43 (Walter de Gruyter, Berlin 2012).

[48] R. Kubo, M. Toda, and N. Hashitsume, *Statistical Physics II: Nonequilibrium Statistical Mechanics* (Springer, Berlin, 1985).

[49] I. Fouxon and M. Holzner, Solvable continuous-time random walk model of the motion of tracer particles through porous media, Phys. Rev. E **94**, 022132 (2016).

[50] K. Alim, S. Parsa, D. A. Weitz, and M. P. Brenner, Local Pore Size Correlations Determine Flow Distributions in Porous Media, Phys. Rev. Lett. **119**, 144501 (2017).

[51] B. Bijeljic, A. Raeini, P. Mostaghimi, and M. J. Blunt, Predictions of non-fickian solute transport in different classes of porous media using direct simulation on pore-scale images, Phys. Rev. E **87**, 013011 (2013).

[52] G. R. Guédon, F. Inzoli, M. Riva, and A. Guadagnini, Pore-scale velocities in three-dimensional porous materials with trapped immiscible fluid, Phys. Rev. E **100**, 043101 (2019).

[53] M. Souzy, H. Lhuissier, Y. Méheust, T. Le Borgne, and B. Metzger, Velocity distributions, dispersion and stretching in three-dimensional porous media, J. Fluid Mech. **891**, A16 (2020).

[54] Bateman Manuscript Project, *Higher Transcendental Functions*, Volume 1 (McGraw-Hill, New York, 1953).

[55] D. A. Benson, R. Schumer, and M. M. Meerschaert, Recurrence of extreme events with power-law interarrival times, Geophys. Res. Lett. **34**, L16404 (2007).

[56] J. Jiménez-Martínez, T. Le Borgne, H. Tabuteau, and Y. Méheust, Impact of saturation on dispersion and mixing in porous media: Photobleaching pulse injection experiments and shear-enhanced mixing model, Water Resour. Res. **53**, 1457 (2017).

[57] P. G. De Gennes, Hydrodynamic dispersion in unsaturated porous media, J. Fluid Mech. **136**, 189 (1983).